



An ultra-thin compact polarization-independent hexa-band metamaterial absorber

Praneeth Munaga¹ · Somak Bhattacharyya² · Saptarshi Ghosh¹ · Kumar Vaibhav Srivastava¹

Received: 14 August 2017 / Accepted: 15 March 2018 / Published online: 23 March 2018
© Springer-Verlag GmbH Germany, part of Springer Nature 2018

Abstract

In this paper, an ultra-thin compact hexa-band metamaterial absorber has been presented using single layer of dielectric. The proposed design is polarization independent in nature owing to its fourfold symmetry and exhibits high angular stability up to 60° angles of incidences for both TE and TM polarizations. The structure is ultrathin in nature with 2 mm thickness, which corresponds to $\lambda/11.4$ (λ is the operating wavelength with respect to the highest frequency of absorption). Six distinct absorption frequencies are obtained from the design, which can be distributed among three regions, namely lower band, middle band and higher band; each region consists of two closely spaced frequencies. Thereafter, the dimensions of the proposed structure are adjusted in such a way that bandwidth enhancement occurs at each region separately. Simultaneous bandwidth enhancements at middle and higher bands have also been achieved by proper optimization of the geometrical parameters. The structure with simultaneous bandwidth enhancements at X- and Ku-bands is later fabricated and the experimental absorptivity response is in agreement with the simulated one.

1 Introduction

Owing to its unusual electromagnetic properties, metamaterials have become the hot topic of research in different applications, viz., lens imaging, cloaking, antenna system and filter [1–5]. Due to the compact nature, metamaterial-based absorbers have found potential applications in different frequency regions from low frequency to optical domain [6–9]. Different types of structures have been proposed as absorbers, viz., electric field-driven LC resonator and closed ring resonator [10–15]. In both the cases, the incident electromagnetic wave has to travel across the thickness of the dielectric over which the patterns are designed. Due to the

high Q nature of the resonators, the absorption bandwidths of these absorbers are quite narrow [11, 12, 16]. To achieve multiple as well as bandwidth-enhanced absorption through metamaterial absorber, many design methodologies have been proposed including array implementation of sub-unit cells as well as single unit cells [15, 17–19], combining multiple unit cells into a single one [12, 20], embedding one unit cell into other [21] as well and stacking of multiple layers into a single unit cell [22, 23]. However, all these approaches suffer from significant increase in terms of the lattice dimension. Potential applications like reduction of radar cross section require compact unit cells capable of achieving multiple absorptions. Recently, structures with quad-band and penta-band absorber applications have also been reported with polarization insensitivity [24–26].

In this paper, a compact solution to achieve hexa-band absorber is presented based on a single thin layer of dielectric substrate. The hexa-band absorber structure has been developed by embedding one compact geometry into another one. The dimensions of the structure have been chosen in such a way that multiple absorption peaks are observed ranging from S- to Ku-bands. The simulated absorption peaks are achieved at 3.16, 4.05, 7.35, 8.65, 11.88 and 13.12 GHz with peak absorptivities of 98.2, 99.5, 99.6, 96.1, 98.9 and 98.8%, respectively. Surface current distributions at all these absorption frequencies are studied to explain the phenomena

✉ Somak Bhattacharyya
bhattacharyya.somak@gmail.com

Praneeth Munaga
praneeth.munaga@gmail.com

Saptarshi Ghosh
joysaptarshi@gmail.com

Kumar Vaibhav Srivastava
kvs@iitk.ac.in

¹ Department of Electrical Engineering, Indian Institute of Technology Kanpur, Kanpur 208016, India

² Department of Electronics Engineering, Indian Institute of Technology (BHU) Varanasi, Varanasi 221005, India

of absorption. The structure has also been investigated with respect to the variation of polarization angle under normal incidence, where it is found to exhibit identical characteristics for any angle of polarization, thus verifying the polarization-independent nature of the structure. Additionally, the design has been studied under oblique incidences for both TE and TM polarizations, and found to have angular stability up to 60° angle of incidence.

The six absorption frequencies of the proposed structure can be categorized into three distinct regions in terms of frequency ranges, viz., lower band, middle band, and upper band, where each band comprises of two closely spaced frequencies. The dimensions of the unit cell are parametrically optimized to achieve bandwidth enhancements at lower band, middle band and higher bands, which are separately placed at S-, X- and Ku-bands, respectively. Furthermore, bandwidth enhancements simultaneously at both X- and Ku-bands have been achieved by proper parametric optimization. The full width at half maxima (FWHM) bandwidth of 0.88 GHz (8.35–9.23 GHz) and 1.2 GHz (12.65–13.85 GHz) has been achieved at X- and Ku-bands, respectively. The designed structure has also been fabricated and absorptivities have been measured experimentally where FWHM bandwidths of 1.59 and 1.16 GHz have been observed at X- and Ku-bands, respectively.

2 Design of the proposed structure

The proposed hexa-band absorber structure is based on two compact geometries embedded in single unit cell imprinted on a dielectric substrate. One of the compact structures is defined as compact absorber I; the top view of whose unit cell is shown in Fig. 1a. The geometrical dimensions of the unit cell are optimized as follows: $a = 15$ mm, $d = 12.6$ mm, $w = 0.4$ mm, $d_1 = 8.8$ mm, $p_1 = 1.5$ mm and $g_2 = 0.2$ mm.

Then, another geometry has been constructed termed as compact absorber II, whose top view of the unit cell is shown in Fig. 1b. The optimized geometrical dimensions are $a = 15$ mm, $d_2 = 7.6$ mm, $p_2 = 1.5$ mm, $w_1 = 0.5$ mm, $g_1 = 0.4$ mm, $g_2 = 0.2$ mm and $gap = 0.3$ mm. Finally, the compact absorber has been designed by embedding compact absorber II inside compact absorber I with geometrical dimensions $a = 15$ mm, $d = 12.6$ mm, $d_1 = 8.8$ mm, $d_2 = 7.6$ mm, $p_1 = 1.5$ mm, $p_2 = 1.5$ mm, $w = 0.4$ mm, $w_1 = 0.5$ mm, $g_1 = 0.4$ mm, $g_2 = 0.2$ mm and $gap = 0.3$ mm. The top view of the unit cell of the overall proposed absorber structure is shown in Fig. 1c. The periodic patterns have been printed on the top surface of a 2-mm-thick FR-4 dielectric of permittivity 4.4 and loss tangent 0.02. The bottom side of the dielectric substrate is completely copper laminated. The directions of the electric field, magnetic field and wave propagation are also shown in Fig. 1a–c.

The absorptivity of the structure can be evaluated from (1), where $A(\omega) = |S_{11}(\omega)|^2$ and $|S_{21}(\omega)|^2$ are the absorptivity, reflected power, and transmitted power, respectively, at an angular frequency ω . Due to the complete copper lamination at the backside, there is no transmitted power ($|S_{21}(\omega)|^2 = 0$). So, by minimizing the reflected power, the absorptivity of the structure is maximized

$$A(\omega) = 1 - |S_{11}(\omega)|^2 - |S_{21}(\omega)|^2 = 1 - |S_{11}(\omega)|^2. \quad (1)$$

3 Simulated results

3.1 Compact absorber I

The unit cell of the compact absorber I shown in Fig. 1a is first simulated using Ansys HFSS for normal incidence of the electromagnetic wave by employing periodic boundary

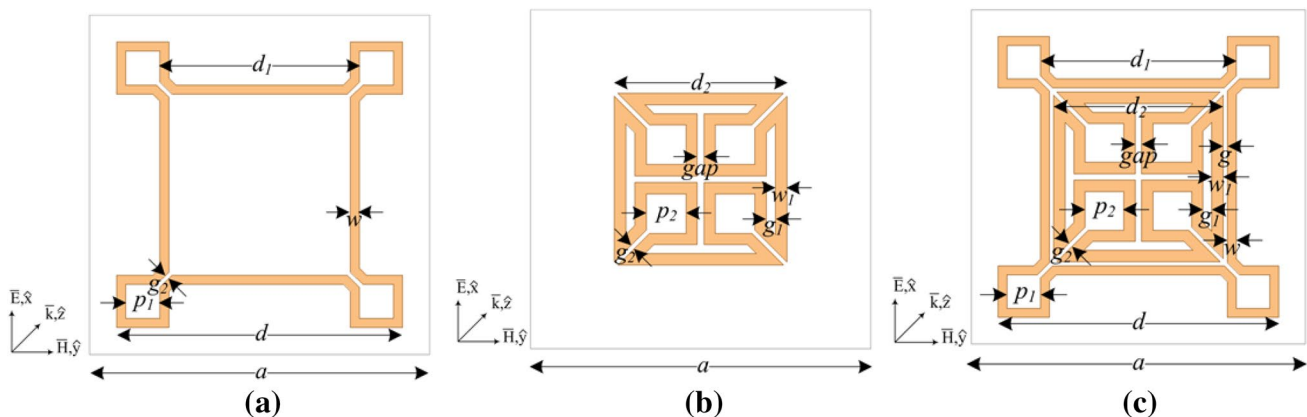


Fig. 1 Top views of the unit cell of the **a** compact absorber I, **b** compact absorber II and **c** proposed compact hexa-band absorber containing absorber II embedded in absorber I

conditions. The absorptivity response of the structure has been shown in Fig. 2, where a simple absorber consisting of simple square loop in a unit cell is also shown. The geometrical dimensions of the square loop are exactly identical with that of the compact absorber I. It is seen that in compact absorber I, absorptions occur at 3.32, 8.72 and 12.84 GHz with peak absorptivities of 92.7, 85.5 and 94.4%, respectively, while the simple absorber with square loop in the unit cell exhibits absorptions at 3.24, 10.88 and 14.80 GHz with peak absorptivities of 79.7, 70.1 and 93.6%, respectively.

The surface current densities at both the top and bottom surfaces of the compact absorber I at frequencies of peak absorptions are shown in Fig. 3. Different regions of the compact absorber I structure are responsible for absorptions at the three distinct frequencies, viz., 3.72, 8.72 and 12.84 GHz. It is seen that the surface currents are anti-parallel at all the frequencies of absorption, thus producing magnetic excitations.

The structure is also studied for different polarization angles of the incident electromagnetic wave under normal incidence as shown in Fig. 4. Due to the fourfold geometrical symmetry of the unit cell, the structure has been studied up to 45° polarization angle. It is seen from Fig. 4 that the absorptivity response remains identical for all angles of polarization, thus making the structure polarization independent in nature.

3.2 Compact absorber II

The compact absorber structure II whose unit cell is shown in Fig. 1b is also simulated using periodic boundary condition and the simulated absorptivity response is shown in Fig. 5. Absorption occurs at 4.28 and 11.70 GHz with peak absorptivities of 97.6 and 40.3%, respectively. Surface current distributions at these two frequencies of absorptions are also illustrated in Fig. 6, where it is seen that different

regions of the absorber structure II get excited at the two distinct absorption frequencies. Here also, the surface currents at top and bottom surfaces are anti-parallel at the two distinct frequencies of absorption, thus confirming the resonance phenomena. The structure has also been studied under polarization angle variations under normal incidence, where the absorptivity response remains invariant as seen from Fig. 7, thus confirming polarization-independent nature of the structure.

3.3 Proposed hexa-band compact absorber

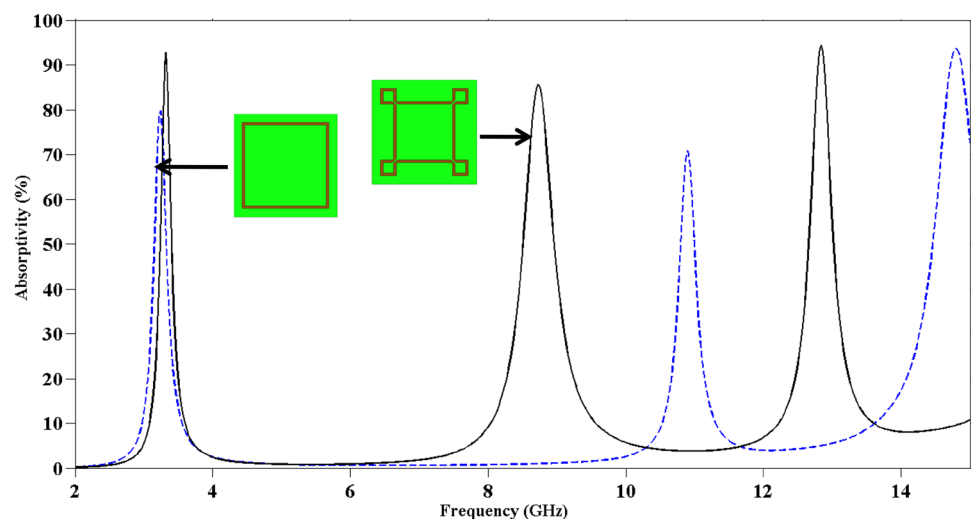
The compact structure I and II are then embedded in single unit cell geometry to obtain the proposed hexa-band absorber as shown in Fig. 1c. The unit cell geometry is simulated in Ansys HFSS using periodic boundary conditions, which results in six distinct absorption peaks occurring at frequencies 3.16, 4.05, 7.35, 8.65, 11.88 and 13.12 GHz with the respective peak absorptivities of 98.2, 99.5, 99.6, 96.1, 98.9 and 98.8%, respectively, as shown in Fig. 8.

The surface current distributions at the peak absorption frequencies are shown in Figs. 9 and 10 at the top and bottom surfaces of the proposed structure. Different regions of the concentric loop are responsible for absorptions as evident from the figures. It is noted that at 8.65 GHz, the coupling between the outer and inner loops produces absorption as seen from Fig. 10.

The structure has also been studied under polarization angle variations. Due to fourfold symmetry of the proposed structure, the absorptivity response has been studied only up to 45° angle of polarizations. The absorptivity remains invariant with the polarization angle variation as evident from Fig. 11, thus revealing the polarization-independent nature of the hexa-band absorber.

The proposed structure has also been studied under oblique incidences till 60° in a step of 5° for both TE and

Fig. 2 Simulated absorptivity response of the compact absorber I with respect to another absorber structure consisting of simple square loop in its unit cell



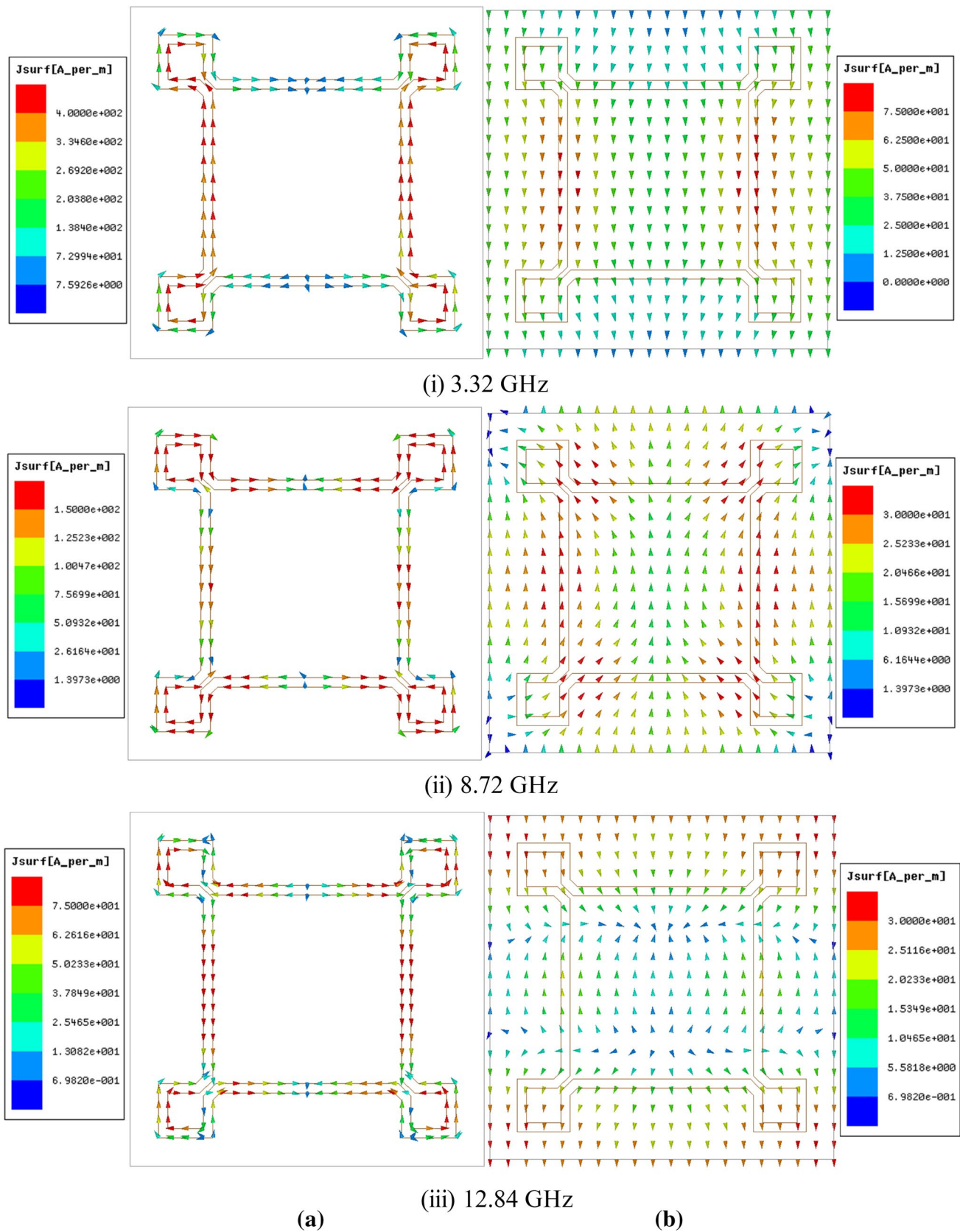


Fig. 3 Surface current distributions at 3.72, 8.72 and 12.84 GHz at **a** top and **b** bottom surfaces of the compact absorber I whose unit cell is shown in Fig. 1a

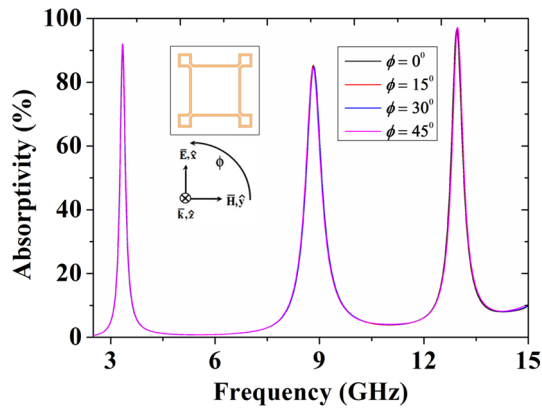


Fig. 4 Absorptivity response of the compact absorber I under various angles of polarization with normal incidence

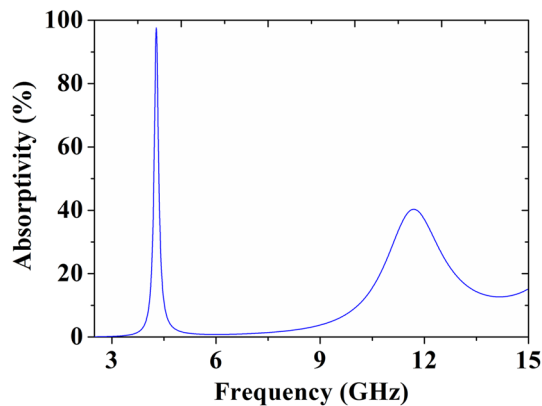


Fig. 5 Absorptivity response of the compact absorber II whose unit cell is shown in Fig. 1b

TM polarizations. In case of TE polarization, the electric field direction remains unchanged, while the directions of magnetic field and wave propagation vector vary. On the contrary, electric field and wave vector direction change and magnetic field direction remains constant during TM polarization. The absorption spectra of the structure under oblique incidences for TE and TM polarizations are shown in Fig. 12a, b, respectively. It is observed that the proposed structure behaves as a hexa-band absorber up to 60° angle of incidences in both the cases. The slight variations of absorptions at higher angular incidence for higher frequencies can be attributed due to the mutual coupling of the resonators [27].

The scattered fields have been studied for oblique incidences over the range 30° – 60° as the diffraction mode is significant for oblique incidences greater than 30° [28, 29] and shown in Fig. 13. It is observed from Fig. 13 that the scattered fields are very less in magnitude and hence can be ignored.

The proposed structure is compact in terms of the dimensions of the unit cell and thickness in comparison to the earlier reported multi-band absorber structures as stated in Table 1. It is also observed from Table 1 that the proposed structure exhibits six distinct absorption peaks using a single unit cell while unit cells of many other multi-band absorber structures are composed of multiple sub-cells.

4 Bandwidth-enhanced absorbers

The proposed structure exhibits six distinct absorption peaks in three different frequency zones, where each zone consists of two closely spaced frequencies, e.g., lower band consists of first two absorption peaks (3.16 and 4.05 GHz), middle band comprises next two absorption peaks (7.35 and 8.65 GHz) and higher band has the last two absorption peaks (11.88 and 13.12 GHz). Bandwidth enhancements at these three distinct zones individually have also been achieved by optimizing geometrical parameters of the unit cell design. Parametric optimization in Ansys HFSS has been carried out for enhancement of the bandwidths in each band.

4.1 Bandwidth enhancement at lower band

A bandwidth-enhanced absorber structure has been obtained by optimizing the geometrical dimensions of the proposed structure as follows: $a = 15$ mm, $d = 13.1$ mm, $d_1 = 10.7$ mm, $d_2 = 8.7$ mm, $p_1 = 0.7$ mm, $p_2 = 2$ mm, $w = 0.5$ mm, $w_1 = 0.45$ mm, $g_1 = 0.64$ mm, $g_2 = 0.5$ mm and $gap = 0.7$ mm. Six distinct absorption peaks are observed in this case along with bandwidth enhancement at lower band. A FWHM bandwidth of 0.35 GHz (3.36–3.71 GHz) in S-band has been achieved, where peak absorptivities of 99.6 and 95.3% are observed at 3.43 and 3.62 GHz, respectively, as shown in Fig. 14. In this case, fractional of 10.2% is realized with respect to frequency with higher absorption peak (3.43 GHz).

4.2 Bandwidth enhancement at middle band

The structure is further optimized to obtain bandwidth-enhanced absorption at X-band. The optimized geometrical dimensions are as follows: $a = 15$ mm, $d = 13.06$ mm, $d_1 = 9.26$ mm, $d_2 = 8.02$ mm, $p_1 = 1.5$ mm, $p_2 = 1.5$ mm, $w = 0.4$ mm, $w_1 = 0.6$ mm, $g_1 = 0.57$ mm, $g_2 = 0.2$ mm and $gap = 0.58$ mm. An enhanced FWHM bandwidth of 0.89 GHz ranging from 7.72 to 8.61 GHz has been obtained as shown in Fig. 15. Two distinct absorption peaks are also observed at 7.94 and 8.51 GHz with peak absorptivities 94.2 and 89.3%, respectively. Here, a fractional bandwidth of 11.2% has been achieved with respect to frequency having higher absorption peak (7.94 GHz).

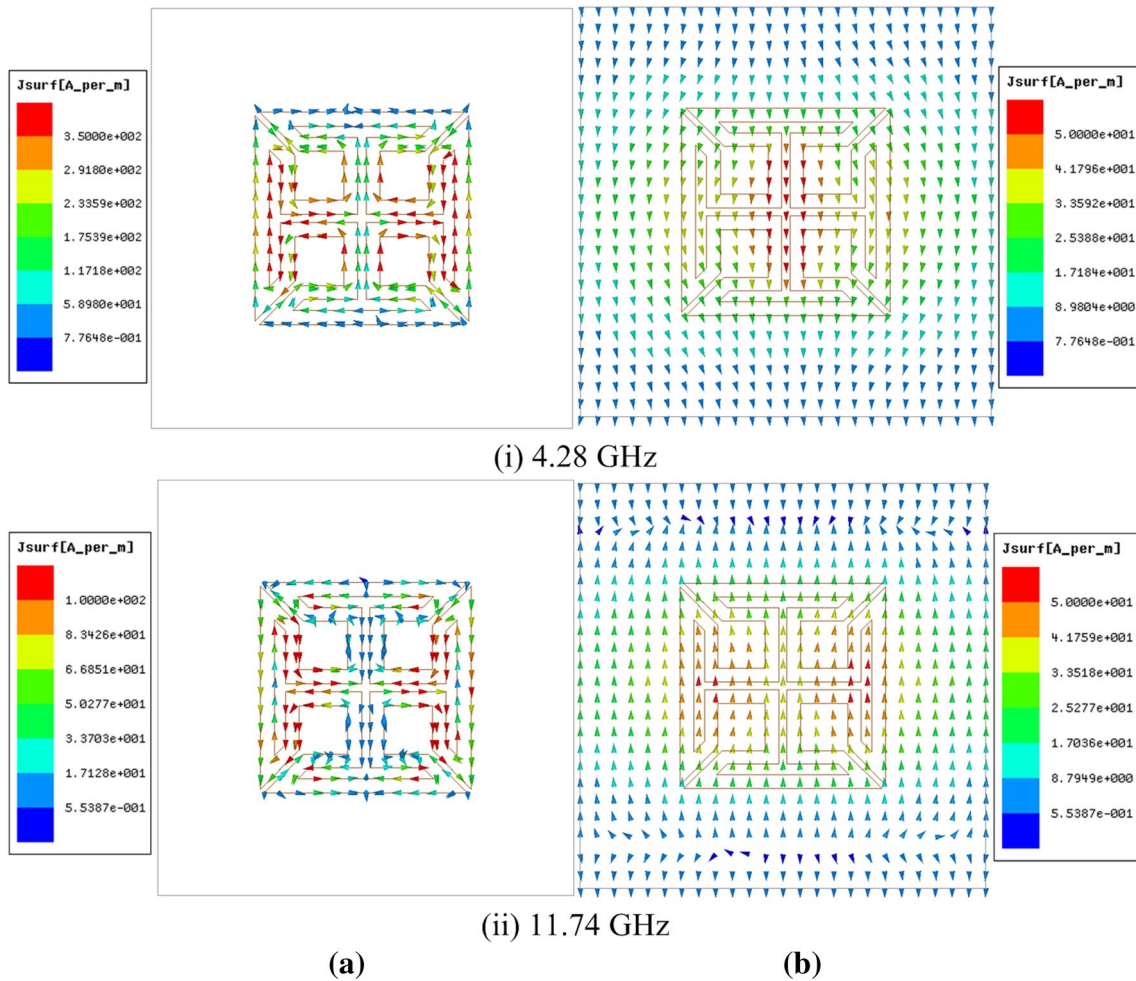


Fig. 6 Surface current distributions at 4.28 and 11.74 GHz at **a** top and **b** bottom surfaces of the compact absorber II whose unit cell is shown in Fig. 1b

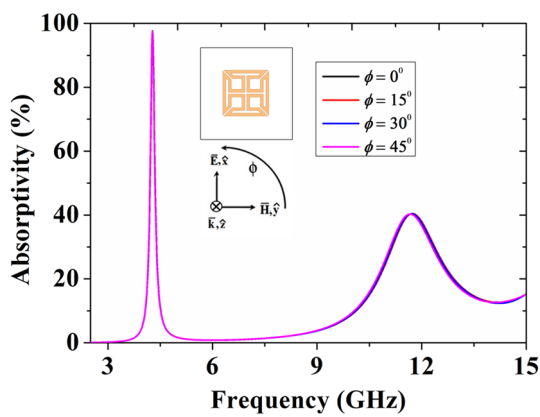


Fig. 7 Absorptivity response of the compact absorber II for various angles of polarization under normal incidence

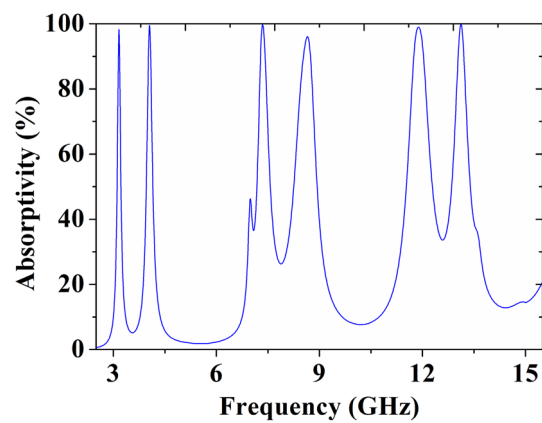


Fig. 8 Simulated absorptivity response of the proposed compact absorber whose unit cell is shown in Fig. 1c

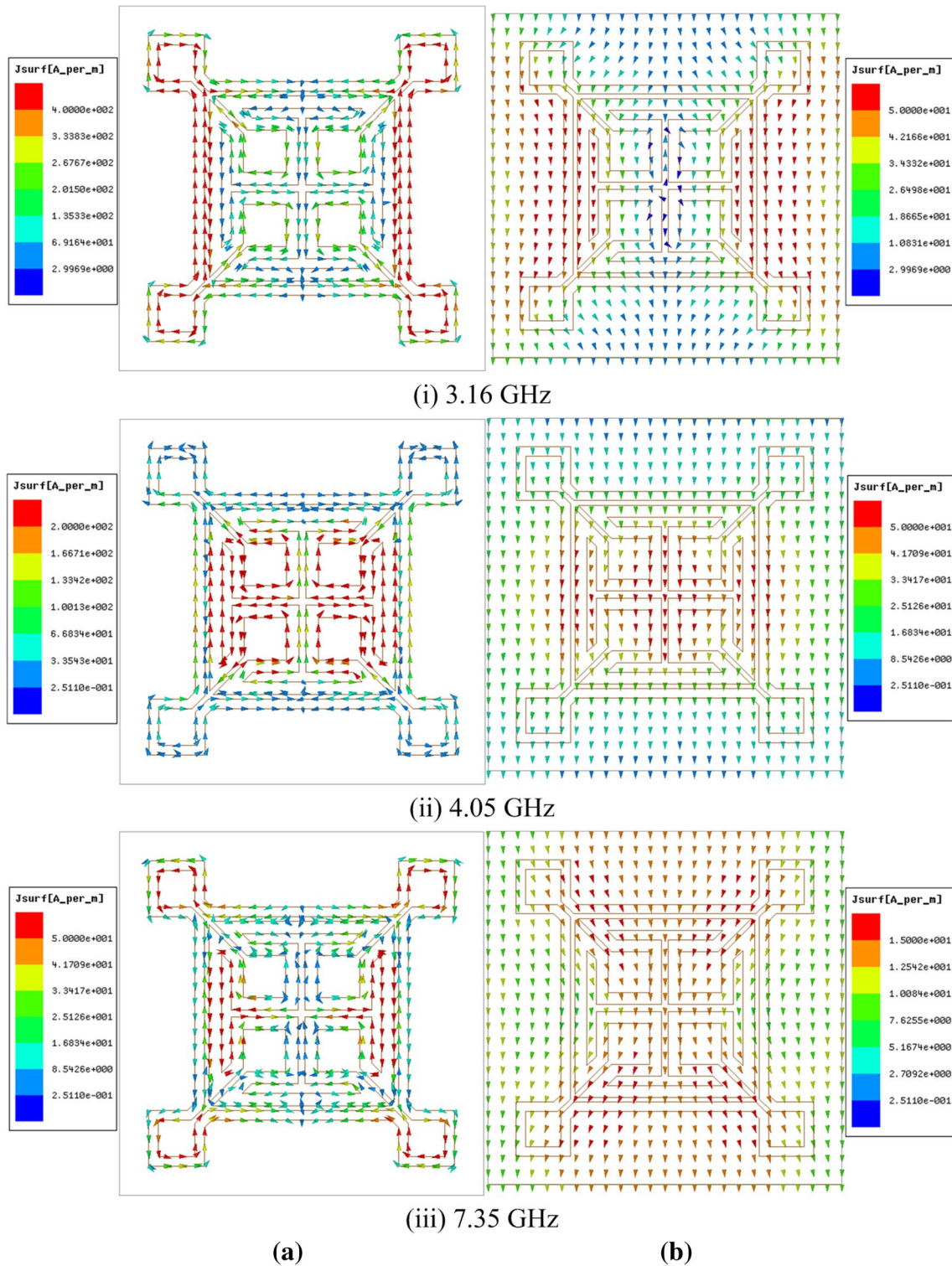


Fig. 9 Surface current distributions at 3.16, 4.05 and 7.34 GHz at **a** top and **b** bottom surfaces of the compact absorber whose unit cell is shown in Fig. 1c

4.2.1 Bandwidth enhancement at higher band

To obtain bandwidth enhancement at higher band, the

geometrical dimensions of the proposed absorber are further modified as: $a = 15$ mm, $d = 12.4$ mm, $d_1 = 8.6$ mm, $d_2 = 7.4$ mm, $p_1 = 1.5$ mm, $p_2 = 1.5$ mm, $w = 0.4$ mm,

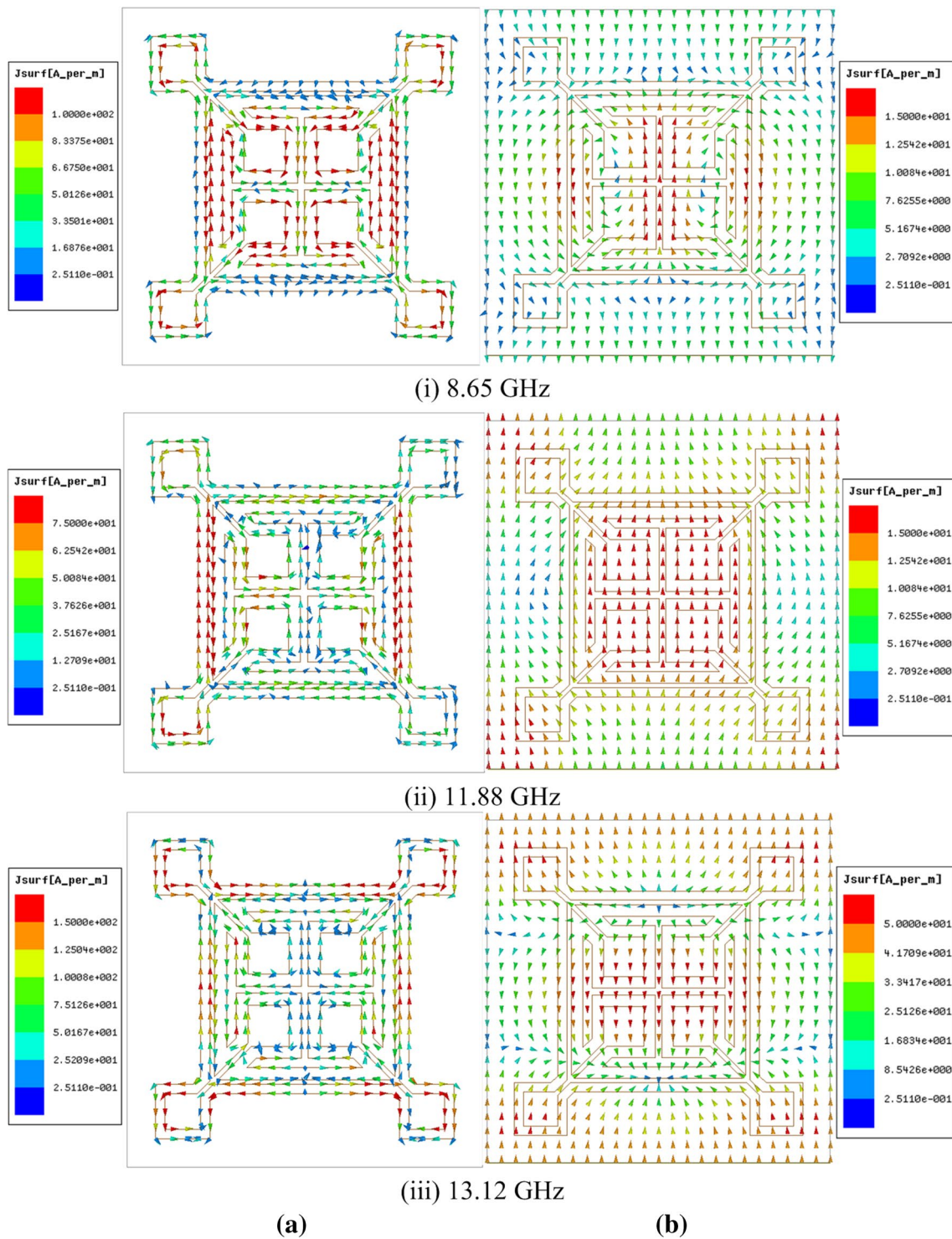


Fig. 10 Surface current distributions at 8.65, 11.88 and 13.12 GHz at **a** top and **b** bottom surfaces of the compact absorber whose unit cell is shown in Fig. 1c

$w_1 = 0.52$ mm, $g_1 = 0.49$ mm, $g_2 = 0.24$ mm and $gap = 0.3$ mm. FWHM bandwidth of 1.41 GHz ranging from 12.38 to 13.79 GHz has been realized at Ku-band along with peak absorptivities of 95.5 and 91.8% at 12.69

and 12.87 GHz, respectively, as shown in Fig. 16. In this case, fractional bandwidth of 11.1% has been realized with respect to 12.69 GHz, the frequency having higher absorption peak.

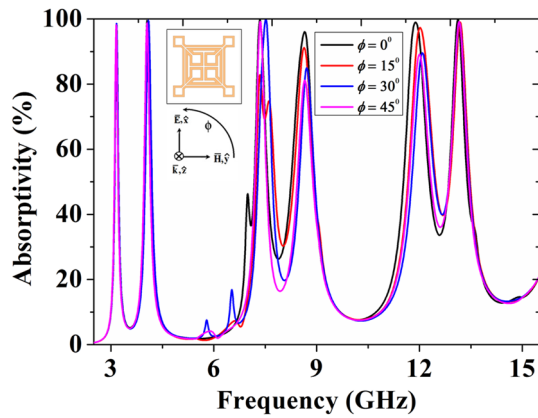


Fig. 11 Absorptivity response of the proposed hexa-band absorber under polarization angle variation with normal incidence

4.3 Simultaneous bandwidth enhancements at middle and higher bands

The geometrical dimensions of the proposed hexa-band absorber have also been modified to attain bandwidth enhancements at middle and higher bands simultaneously. Only the geometrical dimensions $d = 12.11$ mm, $d_1 = 8.31$ mm, $d_2 = 7.11$ mm and $g_1 = 0.38$ mm have been tailored keeping other dimensions unaltered in the hexa-band absorber structure. It is inferred from the simulated absorptivity response that the structure exhibits FWHM bandwidths of 0.88 GHz (8.35–9.23 GHz) at X-band and 1.2 GHz (12.65–13.85 GHz) at Ku-band as shown in Fig. 17. Fractional bandwidths of 9.9 and 8.8% have been realized in X-band and Ku-band, respectively, in this design referring to frequencies with higher absorption peaks, viz., 8.9 and 13.56 GHz.

Since parametric optimization has been done in the geometry of the two resonators individually having three and two absorption peaks, respectively, to obtain enhanced bandwidth absorptions, the notch is due to the effect of coupling between the two resonators nested one between the

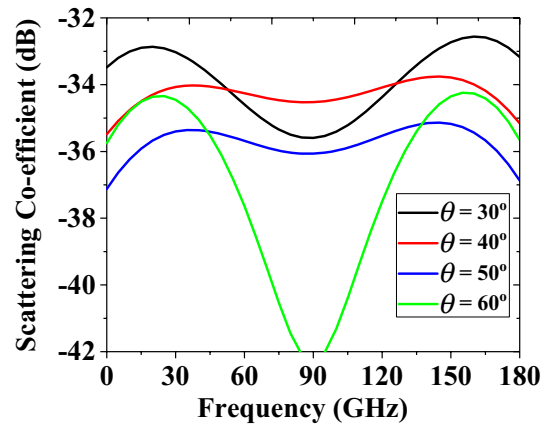


Fig. 13 Frequency response of the scattering coefficient for oblique incidences

other. The individual absorption bands are narrow in nature, having high Q. So, it cannot be improved in this case even with the best possible parametric optimization. At the notch frequencies, minimum absorptions of 60% have been realized for all designs of the unit cells discussed in this section.

5 Experimental verification of the hexa-band absorber with bandwidth-enhanced absorption at middle and higher bands

The proposed compact absorber structure having simultaneous bandwidth enhancements at X- and Ku-bands (discussed in Sect. 4.4) has been fabricated on a 2-mm-thick FR-4 dielectric substrate with dimensions 240 mm × 240 mm with 16 × 16 unit cells using printed circuit board (PCB) technology. The complete fabricated prototype is shown in Fig. 18a while its zoomed view is shown in Fig. 18b.

To measure the experimental absorptivity, the fabricated prototype is kept in an anechoic chamber. Initially,

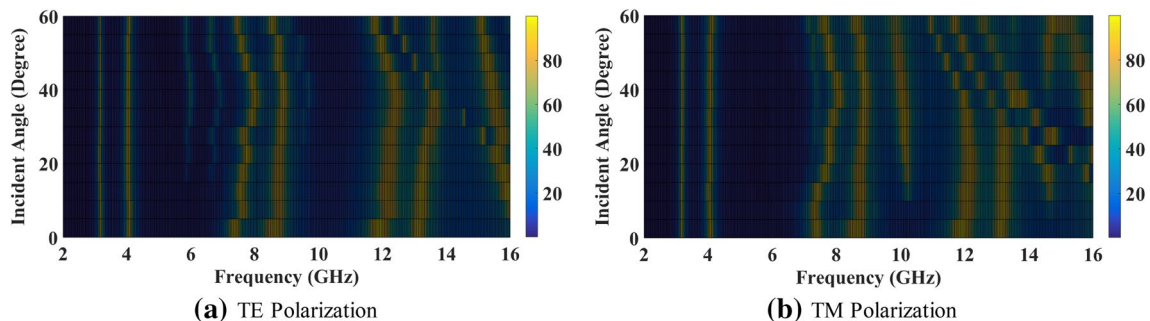


Fig. 12 Absorption spectra of the proposed hexa-band absorber under oblique incidences with a TE polarization and b TM polarization

Table 1 Comparison of the proposed structure with earlier reported multi-band absorbers

Absorber structure	No. of layers	No. of absorption peaks	Unit cell size (with respect to lowest absorption frequency)	Thickness (with respect to lowest absorption frequency)
[30]	1	2	$\lambda_0/2.18$	$\lambda_0/46$
[19]	1	2	$\lambda_0/2.93$	$\lambda_0/29.3$
[10]	1	3	$\lambda_0/3.1$	$\lambda_0/46.1$
[16]	1	3	$\lambda_0/3.1$	$\lambda_0/54.9$
[31]	2	3	$\lambda_0/3.51$	$\lambda_0/63$
[15]	1	4	$\lambda_0/3.2$	$\lambda_0/57.4$
[25]	1	4	$\lambda_0/3.19$	$\lambda_0/49$
[24]	1	4	$\lambda_0/4.9$	$\lambda_0/72$
[26]	1	5	$\lambda_0/6.3$	$\lambda_0/88$
Proposed structure	1	6	$\lambda_0/6.3$	$\lambda_0/47.5$

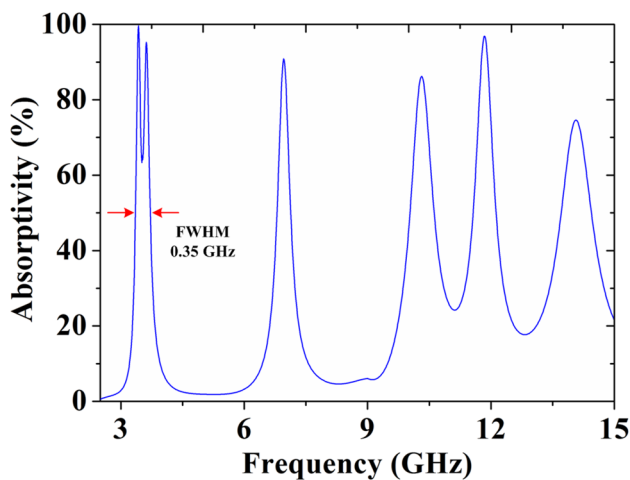


Fig. 14 Absorptivity response of the proposed absorber structure with bandwidth enhancement at lower band (S-band) under normal incidence

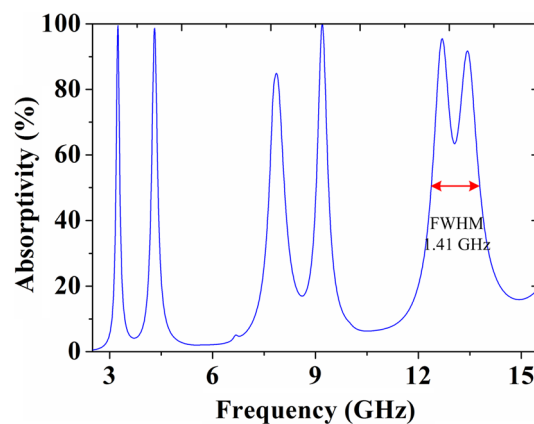


Fig. 16 Absorptivity response of the proposed structure with bandwidth enhancement at higher band (Ku-band) under normal incidence

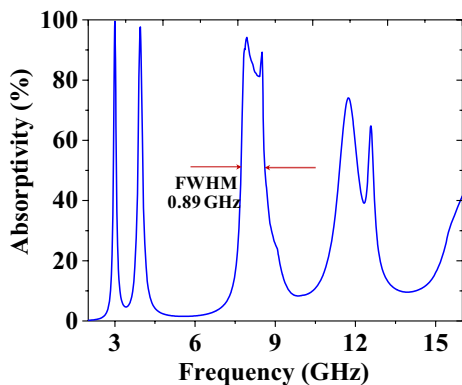


Fig. 15 Absorptivity response of the proposed absorber structure with bandwidth enhancement at middle band under normal incidence

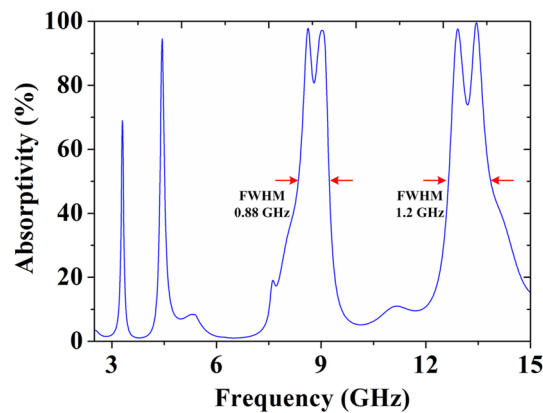


Fig. 17 Absorptivity response of the proposed structure with bandwidth enhancement at middle band (X-band) and higher band (Ku-band) simultaneously under normal incidence

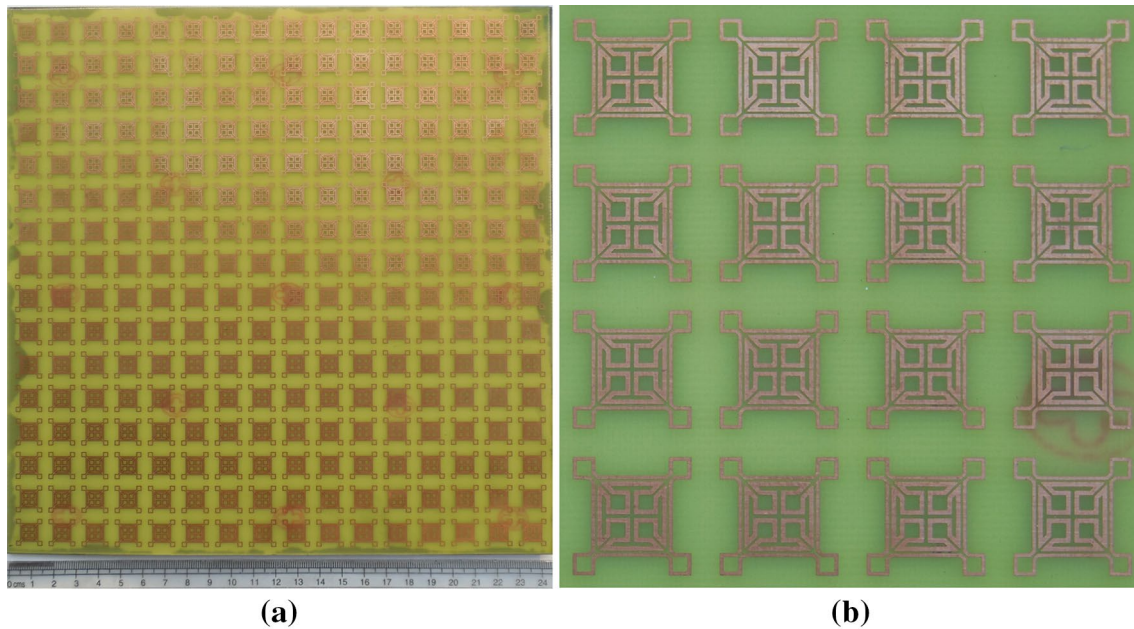


Fig. 18 **a** Complete fabricated prototype of the proposed absorber structure with bandwidth enhancements at middle and higher bands along with **b** its enlarged view

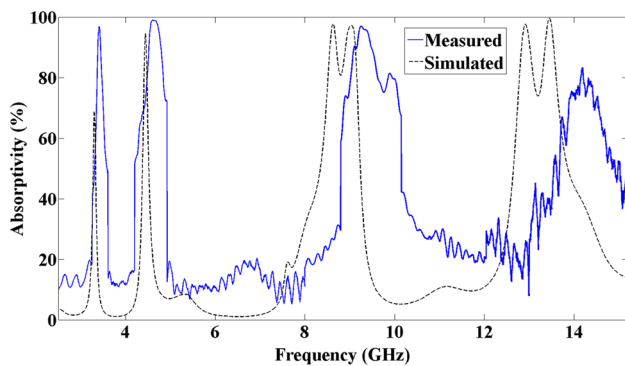


Fig. 19 Comparison of measured and simulated absorption responses of the proposed absorber structure with simultaneous bandwidth enhancement at middle band (X-band) and higher band (Ku-band) under normal incidence

the reflection from a copper surface of identical geometrical dimensions to the absorber structure has been considered as reference. A pair of broadband horn antennas (LB-10180-SF operating in 1–18 GHz) is used to measure the reflected power in this purpose, where one antenna has been used to transmit the power while the other one acts as the receiver. The antennas are connected with a vector network analyzer Agilent N5230A to measure the reflection coefficient of the sample. The reflectivities of the fabricated prototype and the copper plate have been measured separately and the difference between the two gives rise to actual measured reflection coefficient of the structure, which in turn gives

rise to the absorptivity. The measured absorptivity response is shown in Fig. 19 where it is compared with the simulated absorptivity response of the structure. The measured result exhibits FWHM bandwidths of 1.59 GHz (8.56–10.15 GHz) and 1.16 GHz (13.68–14.84 GHz) at X-band and Ku-band, respectively, with absorption peaks realized at 9.26, 9.9, 14.19 and 14.32 GHz corresponding to peak absorptivities 96.9, 81.2, 83.4 and 79.9%. The small deviation between the measured and the simulated responses, particularly at high frequency ranges, are due to the fabrication tolerance and non-linear behavior of dielectric substrate properties. The permittivity and loss tangent of FR-4 structure are functions of frequency in practice. In the simulation, they are assumed to be constant. Thus, slight deviations of absorptivity response at higher frequencies are observed.

6 Conclusions

A compact hexa-band metamaterial absorber has been designed by embedding two compact geometries in single unit cell imprinted on a single layer of dielectric substrate. The proposed hexa-band absorber structure is polarization independent and angularly stable up to 60° incident angles for both TE and TM polarizations. The design has also been optimized in such a way that bandwidth enhancements are obtained at S-, X-, and Ku-bands separately as well as at X-band and Ku-band simultaneously. The measured absorptivity response of the fabricated prototype is also in good

agreement with the simulated response. The proposed structure is suitable for applications including reduction of radar cross section and electromagnetic interference (EMI)/electromagnetic compatibility (EMC).

References

1. D.R. Smith, W.J. Padilla, D.C. Vier, S.C. Nemat-Nasser, S. Schultz, Composite medium with simultaneously negative permeability and permittivity. *Phys. Rev. Lett.* **84**(18), 4184–4187 (2000)
2. N. Fang, H. Lee, C. Sun, X. Zhang, Sub-diffraction-limited optical imaging with a silver superlens. *Science* **308**(5721), 534–537 (2005)
3. S.A. Cummer, B.I. Popa, D. Schurig, D.R. Smith, J.B. Pendry, Full wave simulations of electromagnetic cloaking structures. *Phys. Rev. E* **74**, 036621 (2006)
4. K. Alici, E. Ozbay, Radiation properties of a split ring resonator and monopole composites. *Phys. Stat. Sol. (B)* **244**(4), 1192–1196 (2007)
5. M. Gill, J. Bonache, F. Martin, Metamaterial filters: a review. *Metamaterials* **2**(4), 186–197 (2008)
6. N. Wang, X. Dong, W. Zhou, C. He, W. Jiang, S. Hu, Low-frequency metamaterial absorber with small-size unit cell based on corrugated surface. *AIP Adv.* **6**(2), 025205 (2016)
7. N.I. Landy, S. Sajuyigbe, J.J. Mock, D.R. Smith, W.J. Padilla, Perfect metamaterial absorber. *Phys. Rev. Lett.* **100**, 207402 (2008)
8. H. Tao, N. Landy, C.M. Bingham, X. Zhang, R.D. Averit, W.J. Padilla, A metamaterial absorber for the terahertz regime: design, fabrication and characterization. *Opt. Express* **16**(10), 7181–7188 (2008)
9. N. Zhang, P. Zhou, D. Cheng, X. Weng, J. Xie, L. Deng, Dual-band absorption of mid-infrared metamaterial absorber based on distinct dielectric spacer layers. *Opt. Lett.* **38**(7), 1125–1127 (2013)
10. H. Li, L. Hua Yang, B. Zhou, X. Peng Shen, Q. Cheng, T.J. Cui, Ultrathin multiband gigahertz metamaterial absorbers. *J. Appl. Phys.* **110**(1), 014909 (2011)
11. S. Bhattacharyya, H. Baradiya, K.V. Srivastava, An ultra thin metamaterial absorber using electric field driven LC resonator with meander lines. in *IEEE International Symposium on Antennas and Propagation and USNC/URSI National Radio Science Meeting*, Chicago, 8–13 July, p. 1 (2012)
12. S. Bhattacharyya, K.V. Srivastava, An ultra thin electric field driven lc resonator structure as metamaterial absorbers for dual band applications. in *URSI International Symposium on Electromagnetic Theory (EMTS) 2013*, Hiroshima, Japan, 20–24 May, p. 722 (2013)
13. X. Shen, T.J. Cui, J. Zhao, H.F. Ma, W.X. Jiang, H. Li, Polarization-independent wide-angle triple-band metamaterial absorber. *Opt. Express* **19**(10), 9401–9407 (2011)
14. G. Dayal, S.A. Ramakrishna, Design of multi-band metamaterial perfect absorbers with stacked metal–dielectric disks. *J. Opt.* **15**(5), 055106 (2013)
15. S. Bhattacharyya, S. Ghosh, K.V. Srivastava, Triple band polarization-independent metamaterial absorber with bandwidth enhancement at X-band. *J. Appl. Phys.* **114**(9), 094514 (2013)
16. S. Bhattacharyya, K.V. Srivastava, Ultra thin metamaterial absorbers using electric field driven LC (ELC) resonator structure. in *Progress In Electromagnetics Research Symposium*, Kuala Lumpur, Malaysia, 27–30 March, pp. 314–317 (2012)
17. S. Bhattacharyya, K.V. Srivastava, Triple band polarization-independent ultra-thin metamaterial absorber using ELC resonator. *J. Appl. Phys.* **115**(6), 064508 (2014)
18. S. Ghosh, S. Bhattacharyya, Y. Kaiprath, K.V. Srivastava, Bandwidth-enhanced polarization insensitive microwave metamaterial absorber and its equivalent circuit model. *J. Appl. Phys.* **115**(10), 104503 (2014)
19. S. Ghosh, S. Bhattacharyya, K.V. Srivastava, Bandwidth-enhancement of an ultra-thin polarization insensitive metamaterial absorber. *Microw. Opt. Technol. Lett.* **56**(2), 350–355 (2014)
20. H. Tao, C.M. Bingham, D. Pilon, K. Fan, A.C. Strikwerda, D. Shrekenhamer, W.J. Padilla, X. Zhang, R.D. Averitt, A dual-band terahertz metamaterial absorber. *J. Phys. D Appl. Phys.* **43**, 225102 (2010)
21. S. Bhattacharyya, S. Ghosh, K.V. Srivastava, Equivalent circuit modeling of an ultra-thin polarization-independent triple band metamaterial absorber. *AIP Adv.* **4**(9), 097127 (2014)
22. S. Bhattacharyya, S. Ghosh, D. Chaurasiya, K.V. Srivastava, Bandwidth-enhanced dual-band dual-layer polarization-insensitive ultra-thin metamaterial absorber. *Springer Appl. Phys. A* **118**(1), 207–215 (2015)
23. S. Bhattacharyya, K.V. Srivastava, Dual layer polarization insensitive dual band metamaterial absorber with enhanced bandwidths. in *IEEE Asia Pacific Microwave Conference (APMC) 2014*, Sendai, Japan, 4–7 November, pp. 816–818 (2014)
24. D. Chaurasiya, S. Ghosh, S. Bhattacharyya, A. Bhattacharya, K.V. Srivastava, A compact multi-band polarization-insensitive metamaterial absorber. *IET Microw. Antennas Propag.* **10**(1), 94–101 (2016)
25. N. Wang, J. Tong, W. Zhou, W. Jiang, J. Li, X. Dong, S. Hu, Novel quadruple-band microwave metamaterial absorber. *IEEE Photonics J.* **7**(1), 5500506 (2015)
26. A. Bhattacharya, S. Bhattacharyya, S. Ghosh, D. Chaurasiya, K.V. Srivastava, An ultra-thin penta-band polarization-insensitive compact metamaterial absorber for airborne radar application. *Microw. Opt. Technol. Lett.* **57**(11), 2519–2524 (2015)
27. S. Ghosh, K.V. Srivastava, An equivalent circuit model of FSS-based metamaterial absorber using coupled line theory. *IEEE Antennas Wirel. Propag. Lett.* **14**, 511–514 (2015)
28. S.R. Seshadri, Diffraction grating for the general oblique incidence. *J. Appl. Phys.* **69**, 574 (1991)
29. W. Shang, W. Zhang, J. Yang, T. Zhu, L. Kuang, S. Li, Influence of oblique incidence on transmission grating diffraction in soft X-ray region. *Mater. Express* **2**, 151–156 (2012)
30. M.-H. Li, H.-L. Yang, X.-W. Hou, Perfect metamaterial absorbers with dual bands. *Prog. Electromagn. Res.* **108**, 37–49 (2010)
31. L. Huang, H. Chen, Multi-band and polarization insensitive metamaterial absorber. *Prog. Electromagn. Res.* **113**, 103–110 (2011)